10.24425/acs.2022.143667

Archives of Control Sciences
Volume 32(LXVIII), 2022
No. 4, *pages* 677–707

Improved Matlab/Simulink model of dual three-phase fractional slot and concentrated winding PM motor for EV applied brushless DC drive

Ihor SHCHUR, Damian MAZUR, Olekcandr MAKARCHUK, Ihor BILYAKOVSKYY, Valentyn TURKOVSKYI, Bogdan KWIATKOWSKI and Dawid KALANDYK

The development of electric vehicles (EV) necessitates the search for new solutions for configuring powertrain systems to increase reliability and efficiency. The modularity of power supplies, converters, and electrical machines is one such solution. Among modular electric machines, dual three-phase (DTP) motors are the most common in high-power drives. To simplify low and medium power drives for EVs based on DTP PM motor, it is proposed to use a BLDC drive and machine of the simplest design – with concentrated windings and surface mounted PMs on the rotor. To study and create such drives, an improved mathematical model of DTP PM machine was developed in this work. It is based on the results of 2D FEM modeling of the magnetic field. According to the developed method, the dependences of the self and mutual inductances between all phase windings from the angle of rotor position and loads of different motor modulus were determined. Based on these inductances, the circuit computer model of DTP PM machine was created in the Matlab/Simulink. It has a high simulation speed and a high level of adequacy, which is confirmed by experimental studies with a mock-up sample of the electric drive system.

Key words: electric vehicle (EV), dual three-phase (DTP) motor, BLDC drive, fractional slot concentrated winding PM motor, FEM modeling, self and mutual differential inductances, Matlab/Simulink model

I. Shchur (e-mail: ihor.z.shchur@lpnu.ua), O. Makarchuk (e-mail: oleksandr.v.makarchuk@lpnu.ua), I. Bilyakovskyy (e-mail: ihor.y.biliakovskyi@lpnu.ua) and V. Turkovskyi (e-mail: valentyn.p.turkovskyi@lpnu.ua) are with Department of Electric Mechatronics and Computer-Controlled Electromechanical Systems, Lviv Polytechnic National University, Lviv 79013, Ukraine.

D. Mazur (corresponding author, e-mail: mazur@prz.edu.pl) and B. Kwiatkowski (e-mail: b.kwiatkowsk@prz.edu.pl) are with Department of Electrical Engineering and Fundamentals of Computer Science, Rzeszow University of Technology, Rzeszow 35-959, Poland.

D. Kalandyk (e-mail: d548@prz.edu.pl) is with Doctoral School of Engineering and Technical Sciences at the Rzeszow University of Technology, Rzeszów 35-959, Poland.

O. Makarchuk (e-mail: oleksandr.makarchuk@pcz.pl) is also with Faculty of Electrical Engineering, Czestochowa University of Technology, Częstochowa 42-200, Poland.

Received 12.03.2022. Revised 11.09.2022.

1. Introduction

The main cause of environmental problems in recent decades, such as global warming and air pollution, is the long-term use of fossil fuels, much of which are consumed by vehicles. In recent years, significant efforts have been made to change the situation in the direction of reducing air pollution from transport. Electrification technologies of existing vehicles are increasingly progressed, first, full and hybrid electric vehicles (EV and HEV) are developed, and new groups of vehicles are created, in particular, in the part of individual low-power vehicles and mobile robots for various purposes [1]. The environmental friendliness of EVs is determined by two factors: (i) the division in time, space and capacity of the processes of electricity generation and its consumption to ensure traffic, (ii) the widespread use of electricity produced from renewable sources. As EVs become a key trend in transport technologies, their main requirements are efficiency and reliability [2].

These two indicators can be significantly increased by applying a modular approach in the construction of power supplies, power converters and the electric machines themselves [2–4]. Among the latter, multiphase electric machines, which have become the subject of considerable interest over the past two decades, fit well into the concept of the modular approach. The advantages of multiphase machines include reduced ripple of the electromagnetic torque, reduced content of current harmonics in the DC link, potentially higher efficiency, reduced power per phase, significantly improved reliability and increased robustness to failure [5–7]. One of the new promising solutions for electric transport in the field of multiphase electric machines is the use of separate groups, often two, three-phase (DTP) windings, which are connected to separate two-level voltage source inverters (VSI) powered by separate modules of onboard power supplies. Compared to traditional drives with one three-phase winding, DTP motor drives are inherently fault tolerant, as a failure of one module does not result in complete loss of control of the vehicle. The popularity of this type of machine follows from the good trade-off between additional complexity and potential advantages [5, 8–10].

In the DTP machines, the vectors of magneto-motive forces (MMF) of two groups of windings can coincide in direction (symmetrical configuration) or be shifted by a certain angle (asymmetric configuration) [5, 9, 10]. The asymmetric DTP machine (see Fig. 1) has two sets of three-phase stator windings, 1-2-3 and 4-5-6, spatially shifted by 30°el. with isolated neutral points or modules of power supply, which eliminates the pulsating electromagnetic torque of the sixth harmonic. This configuration is also known in the literature as an asymmetric six-phase machine, a divided-phase machine or a double star machine. Until recently, such an implementation of the power circuit was used only in high-power

asynchronous medium-voltage electric drives. However, recently, the DTP configuration has been extended to synchronous machines with permanent magnets (PMSM), including for EVs drives [8, 11].

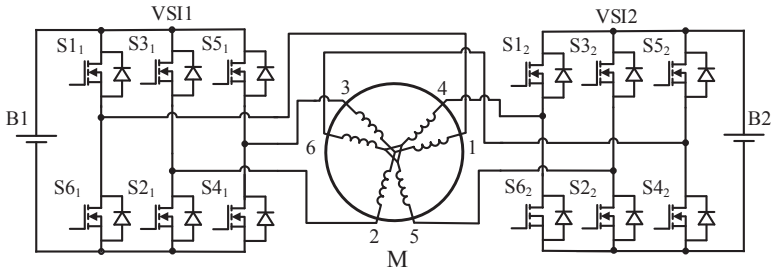

Figure 1: Asymmetric DTP configuration of the electric drive

In PMSM DTP drive, control of each module is provided by a separate voltage source inverter, VSI1 and VSI2 in Fig. 1, which are synchronized to the current position of the rotor utilizing sensors of the rotor angular position. In this case, the execution of the armature magnetic circuit can be magnetically insulated for each module or common to both modules of the machine. Since in the latter case, much higher specific values of torque and power are achieved, it is most often used. In order to implement a large number of individual phase windings and reduce losses in their end winding parts, concentrated windings with non-intersecting winding end parts are most often used in multiphase PMSMs. In this case, to reduce the mutual inductive connections between the modules of the armature winding and the electromagnetic torque ripple, the fractional ratio of the number of turns per pole and phase is used [12]. Fractional-slot concentrated winding has a number of advantages over distributed windings in traditional machines, such as high winding factor, high copper packing factor, short end windings, and hence, high efficiency, reduction in the likelihood of an interphase fault, and extremely low cogging torque [13]. However, fractional-slot windings still generate a large number of space harmonics in the stator MMF, which rotate at different speeds relative to the rotor and hence cause many undesirable effects that include localized core saturation, eddy-current losses in the permanent magnets, acoustic noise, and vibrations.

The prospect of using the DTP PMSMs for EVs determines the relevance of research on mathematical modeling of their work and the development of ways to control them. In particular, the difficulty in modeling electromagnetic processes is to take into account the mutual magnetic influence between the windings of both machine modules. In the case of modules with sinusoidal MMF distribution and sinusoidal armature currents, the electromagnetic processes in DTP PMSM can be quite well described in two d-q rotor reference frames with a mutual electromagnetic coupling [14, 15]. Self and mutual inductances of the armature

windings are obtained by simulating the electromagnetic field of the machine by the finite element method (FEM) and describe their dependences on the rotor position using different numbers of coefficients. Then, using special coordinate transformations, we obtain a mathematical description of electromagnetic processes in DTP PMSM in two decoupled d-q rotor reference frames [16]. In these coordinate systems, vector control of module currents is built, and an important task is the power or current sharing among three-phase winding sets [17]. A productive method of such modeling and control is the vector space decomposition (VSD) method, which provides high-quality separation of cross coupling between reference frames and allows implementing measures to reduce current harmonics [18].

The performance of a high-quality modular electric drive based on DTP PMSM is associated with significant hardware and software complexity of the entire system, which can be justified only for powerful and expensive EVs. However, the above advantages of the DTP concept will be effective for simpler and cheaper vehicles of lower power. A significant simplification of the modular configuration for such applications is the transition to brushless DC motor (BLDCM) with the known advantages of this drive in the application of a simpler design of an electric machine with PMs placed on the rotor surface, cheap point sensors of the angular rotor position, low-frequency switching of the armature winding [19]. However, in this case, the modules of the electric machine are characterized by a clear non-sinusoidal MMF, due to both spatial and temporal harmonics of flux linkages. As far as the authors know, few works have been devoted to modeling electromagnetic processes in DTP BLDCM [20–26]. In these works, the electromagnetic processes in the modules of machines are described by circular equations of voltage balances taking into account the magnetic relationships between the phases of each module and between the two modules. In [20–25], the authors applied a simple modeling of self and mutual inductances by constant, independent of rotor position, quantities and focused on the issue of uniform current distribution between the machine modules and the development of control systems. The approach to mathematical modeling used in [26] is characterized by special accuracy, but the developed complex mathematical model cannot be used for fast simulation, which is necessary for the study of different structures of control systems.

In this work, the research was conducted in the direction of mathematical modeling of the DTP PM machine. The dependences of the total flux linkages of the electrical circuits and the electromagnetic torque on the currents in these circuits and the rotor position angle were determined by numerical simulation using 2D FEM. According to the developed method, for different variants of module loads, the dependences of the self and mutual inductances on the rotor position angle were determined. Based on the obtained results, a mathematical model of DTP PM machine in-phase reference frames is constructed, which allows finding the corresponding components of the armature currents by integrating six

differential equations, and then calculating the current value of electromagnetic torque from the obtained current values. The complete dynamic model of the studied electric machine is implemented in the Matlab/Simulink environment. The created with accepted assumptions computer model has a relatively higher level of adequacy and high speed for simulation on a personal computer. The time dependences of the armature currents of the individual modules obtained on the computer model were compared with the corresponding oscillograms taken experimentally on the mock-up sample of the BLDC drive system. The convergence of theoretical and experimental results was quite satisfactory that indicates the adequacy of the developed model. Its application in further research allows to estimate the magnitude of the electromagnetic torque ripple by results of computer simulation and to develop electric drive systems based on DTP BLDCM for different EVs.

2. FEM-analysis of the electromagnetic part of the studied DTP PM machine

To analyze DTP PM machine, we propose to use one of the fundamental concepts of the nonlinear theory of electromechanical energy conversion, namely the concept of magnetic mechanical characteristic (MMC) – the dependence of total flux linkages of electrical circuits and generalized forces (electromagnetic torque) on currents in these circuits and generalized displacements (rotor position angle) [27]. Partial derivatives of MMS on the vector of currents and the angle of the rotor position, the so-called magnetic mechanical parameters (MMP), give complete information about the angular dependences of the self and mutual differential inductances.

2.1. Determination of the MMCs for the studied DTP PM machine

The total flux linkage of any electrical circuit of the stator is the algebraic sum of the flux linkage due to the working flux in the stator slot part of a machine, and the flux linkage due to the leakage flux in the winding end parts. The latter will depend linearly on the currents of all electrical circuits and are the product of the corresponding leakage inductances for these currents. Traditional methods of calculating the leakage inductances of frontal machine parts are used, which are not considered here.

The part of the flux linkage caused by the flux in the slot part of the stator is the product of some elementary magnetic fluxes coupled to the part of the coil and the number of turns contained in this part of the coil. Figure 2 shows a concentrated stator coil wound on a tooth. We divide the regions occupying the sides of the coil into j elementary subdomains, within which we will assume that the magnitude and direction of the magnetic induction vector $\bar{B}$ are constant. Two such subregions S_j are shown in the Fig. 2.

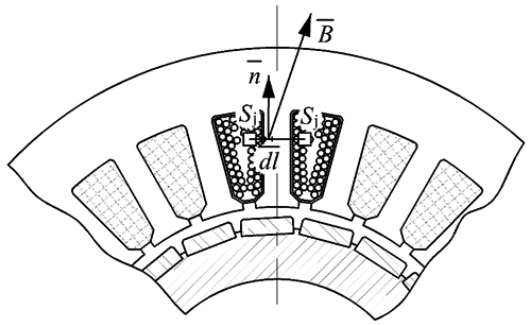

Figure 2: To calculate the total flux linkage of the coil

The flux linkage of the part of the coil bounded by the area S_j is calculated as

$$\psi_j = w_{S_j} l_\delta \int_l \bar{B}\bar{n}\,\mathrm{d}\bar{l}\,, \tag{1}$$

where w_{sj} is the number of turns belonging to the subsquare S_j, l_δ is the calculated length of the magnetic circuit, and $\bar{n}$ is the unit vector (orth) of the normal to the elementary section $d\bar{l}$.

Summing the flux linkage (1) by the area of the slot occupied by the coil, we obtain the flux linkage of the coil due to the flux in the winding part end of the machine:

$$\psi_{\delta km} = \sum_{j=1}^{J} \psi_j\,. \tag{2}$$

The flux linkage of the whole phase $\psi_{\delta m}$ ($m = 1, \ldots, 6$), where m is the current circuit number (phase) of the stator, due to the flow in the slot part, is found as the algebraic sum of the flux linkages of K coils belonging to the circuit with number m. Finally, we obtain complete flux linkages of the stator circuits, which in matrix form are written as

$$\vec{\psi} = L_\sigma \vec{i} + \vec{\psi}_\delta\,, \tag{3}$$

where $\vec{\psi} = \|\psi_1\ \psi_2\ \psi_3\ \psi_4\ \psi_5\ \psi_6\|^T$ is the vector-column of complete flux linkages of electrical circuits of the stator, $\vec{i} = \|i_1\ i_2\ i_3\ i_4\ i_5\ i_6\|^T$ is the vector-column of stator currents, L_σ is the square matrix of inductances of frontal linkage of size 6, and $\vec{\psi}_\delta = \|\psi_{\delta 1}\ \psi_{\delta 2}\ \psi_{\delta 3}\ \psi_{\delta 4}\ \psi_{\delta 5}\ \psi_{\delta 6}\|^T$ is the vector-column of flux linkages of electrical circuits caused by fluxes in the frontal parts of the machine.

The calculation of electromagnetic forces and torque is performed using the so-called Maxwell stress tensor. According to this method, the force acting on

any part of the volume V limited by the surface S can be obtained by summing the elementary forces $d\bar{F} = \bar{F}_n d\bar{S}$ attached to the elements $d\bar{S}$ of the surface S, where $\bar{F}_n$ is the force acting from the outside on the elementary surface.

In a two-dimensional formulation, the vector of the resulting force is calculated as

$$\vec{F} = \frac{1}{\mu_0} \int_l T_m \bar{n} \, \mathrm{d}\bar{l}, \tag{4}$$

where $T_m = \begin{Vmatrix} \frac{1}{2}\left(B_x^2 - B_y^2\right) & B_x B_y \\ B_x B_y & \frac{1}{2}\left(-B_x^2 + B_y^2\right) \end{Vmatrix}$ is the Maxwell's stress tensor for an isotropic medium, B_x and B_y are the projections of the magnetic induction vector on the surface S, and μ_0 is the vacuum permeability.

Based on (4), after simple transformations, the electromagnetic torque, acting on the rotor of an electric machine, is defined as

$$T_e = \bar{z} \cdot \frac{1}{\mu_0} \int_l \bar{r} \times \left[\left(\bar{n} \cdot \bar{B}\right) \cdot \bar{B} - \frac{1}{2} \left(\bar{B} \cdot \bar{B}\right) \cdot \bar{n} \right] \mathrm{d}\bar{l}, \tag{5}$$

where $\bar{z}$ is the unit vector along the axis of rotation and $\bar{r}$ is the radius-vector, which the end belongs to the outer surface of the rotor ($\times$ is the vector product and $\cdot$ is the dot product).

Given the accepted notation (3), we obtain the MMC for DTP PM machine in vector form as

$$\vec{\psi} = \vec{\psi}\left(\vec{i}, \gamma\right), \qquad T_e = T_e\left(\vec{i}, \gamma\right), \tag{6}$$

where γ is the rotor position angle.

The developed algorithm for solving the problem of calculating the MMC values for DTP PM motor by quasi-stationary approximation of the magnetic field in a 2D setting is described in detail in [28]. It involves the performance of calculations, geometric constructions, transformations of coordinate systems, etc., which are performed in two stages: (1) creation of a FEM model of the DTP PM motor, (2) calculation of one value of the MMC. The algorithm is implemented as a computer program using the ANSYS Multiphysics FEM analysis package and the Ansys Parametric Design Language, which is built into the ANSYS.

For research, the DTP PM motor with an external rotor, which can work as a part of an in-wheel motor of some vehicle, is taken. The stator winding of such a machine contains two 3-phase modules, the resulting MMFs of which are shifted by 30° el. The main dimensions of the active part of the machine are shown in Fig. 3a, the number of poles of the inductor $2p = 20$, the number of slots of the stator $Z = 24$, the coils are concentrated. Thus, the condition of fractional

slot concentrated winding is fulfilled. A fragment of the 2D FEM model of the machine magnetic field is shown in Fig. 3b.

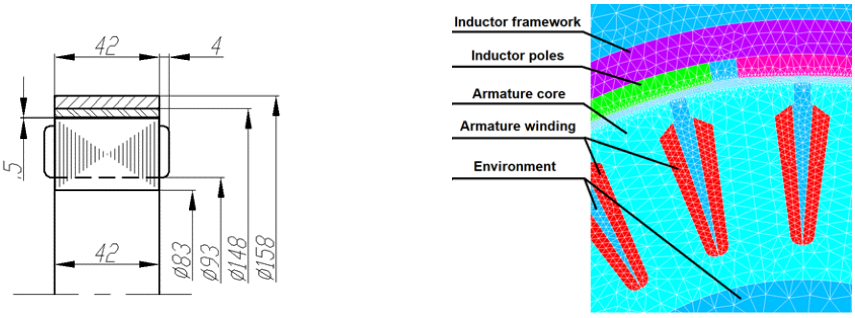

(a) (b)

Figure 3: Dimensions of the active part of the studied DTP PM motor (a) and the fragment of its 2D grid of the FEs (b)

Using the described algorithm for the studied DTP PM machine, the dependences of phase flux linkages on the rotor angle position within the angle of 2π rad el. for the no-load mode are calculated and shown in Fig. 4, where ψ_1, ψ_2, ψ_3 are the phase flux linkages of the first module of the machine and ψ_4, ψ_5, ψ_6 are the flux phase linkages of the second machine module. Based on these phase flux linkages, the corresponding dependences of the EMFs of rotation are obtained, the harmonic composition of which is shown in Fig. 5. From the latter, it is seen that the studied DTP PM machine has fairly close to the sinusoidal form of the EMF of rotation. Only the third harmonic of the EMF is significant and its amplitude is 9.3% of the first harmonic, and the amplitude of the higher harmonics is not more than 1%.

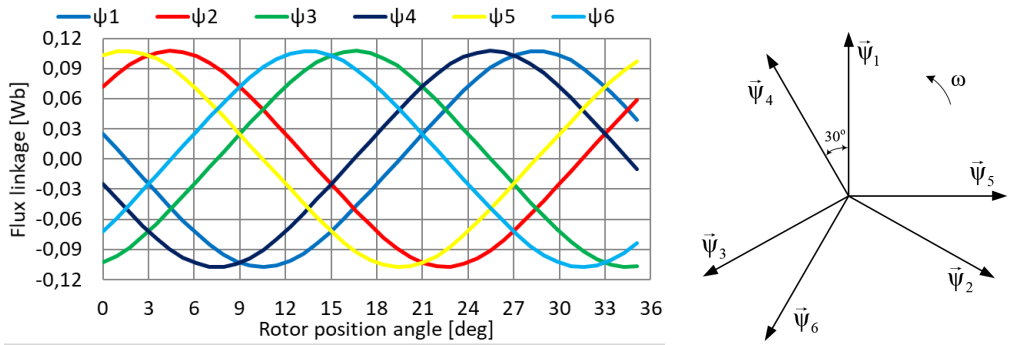

(a) (b)

Figure 4: The obtained dependences of the flux linkages of the studied DTP PM machine on the angle of the rotor position during idling (a) and their vector diagram (b)

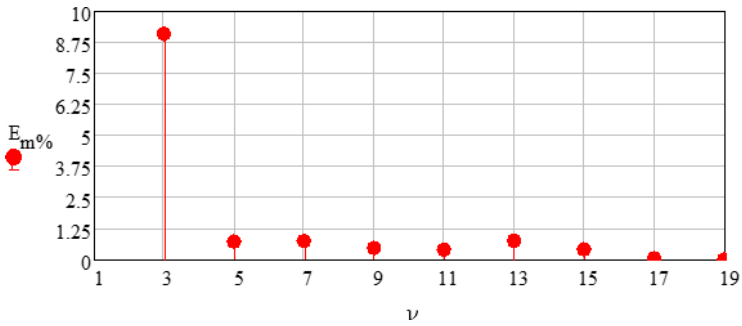

Figure 5: Harmonic composition of the EMF of the studied DTP PM machine

To study the magnetostatic mode, the modular armature winding sets of the machine were fed by symmetrical 3-phase or 2x3-phase sinusoidal current systems, which were synchronized with the phase EMFs of the respective modules in idle mode [28]. The calculations showed the local saturation of the toothed zone, which can be seen from the comparison of the distributions of the magnitudes of the magnetic induction vector during idle and under the load current at the magnitude of 12 A (Fig. 6). The consequence of this is an increase in the amplitudes of the higher harmonics of the magnetic field in the air gap, which, in turn, leads to an increase in the pulsation of the electromagnetic torque.

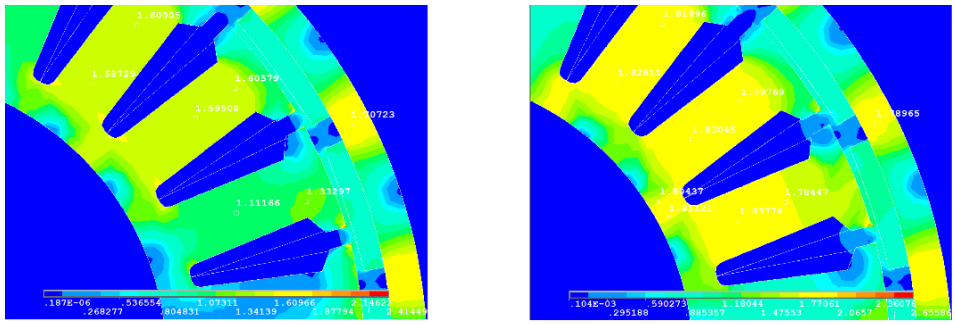

(a) (b)

Figure 6: The field of the magnetic induction vector: (a) idle, (b) the armature current in both winding sets at the magnitude of 12 A

According to the developed algorithm, the MMC for the studied DTP PM machine is constructed. As an example of the calculation results, Fig. 7 graphically shows the dependences of the eponymous phase flux linkages ψ_1, ψ_4 of two machine modules and the electromagnetic torque T_e on the current in the armature phase i_1 for two values of the rotor position angle.

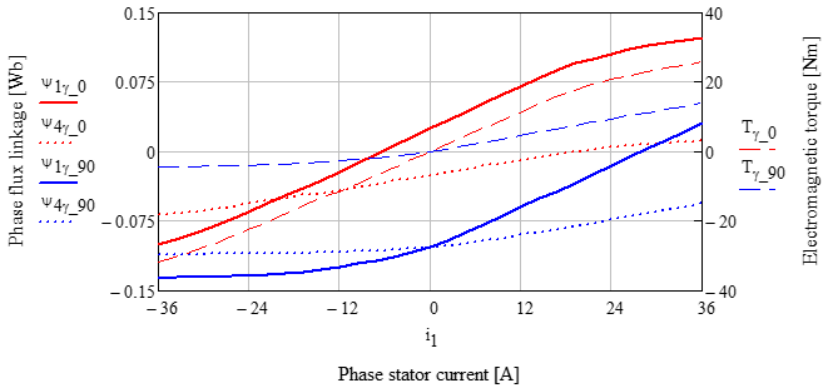

Figure 7: Dependences of the phase flux linkages ψ_1, ψ_4 and the electromagnetic torque T_e on the current i_1 magnitude for two values of the rotor position angle $\gamma = 0$ and $\gamma = 90°$el

Analysis of the obtained results allows us to state the following:

- the same magnitude of the armature current, depending on the rotor position, can increase or decrease the flux linkage of the windings, therefore, magnetizes or demagnetizes the machine;
- the shape of the total flux linkage of the phase windings of one module is determined, first, by its current load, and also depends on the current load of another module;
- the mutual inductive connection between the phases belonging to one module is practically absent;
- the mutual inductive connection between the phases belonging to different modules may have different magnitude and a sign depending on the phase pairs;
- the proportional relationship between the electromagnetic torque and the current is broken by exceeding the load currents of 10–12 A.

2.2. Determination of self and mutual inductances (MMPs) of the studied DTP PM machine

Numerical integration of the system of algebraic-differential equations that describes the transients in the DTP PM machine requires finding the partial derivatives of MMC by the vector of currents and the angle of the rotor position, the so-called MMPs.

From the theory of mathematical modeling of electromechanical energy converters, it is known that the complete derivative of explicit MMC by the argument

of this characteristic is represented in the form of a matrix [29]

$$\frac{\partial\left(\vec{\psi}, T_e\right)}{\partial\left(\vec{i}, \gamma\right)} = \begin{Vmatrix} \dfrac{\partial\vec{\psi}}{\partial\vec{i}} & \dfrac{\partial\vec{\psi}}{\partial\gamma} \\ \dfrac{\partial T_e}{\partial\vec{i}} & \dfrac{\partial T_e}{\partial\gamma} \end{Vmatrix} = \begin{Vmatrix} \boldsymbol{L} & \boldsymbol{K} \\ \boldsymbol{K}' & \boldsymbol{G} \end{Vmatrix}. \tag{7}$$

In our further studies, only the $\boldsymbol{L}$ part of the matrix (7) will be used, which corresponds to the differential inductances of the machine. In the case of the DTP PM machine, matrix $\boldsymbol{L}$ has the size 6×6, the rows of which are partial derivatives of each element of the vector of flux linkage on all line currents of two sets of the armature winding:

$$\boldsymbol{L} = \frac{\partial\vec{\psi}}{\partial\vec{i}}. \tag{8}$$

Since the MMC is a nonlinear vector function of a vector argument, which values are determined based on the calculation of the magnetic field, the analytical finding of the partial derivatives (8) is practically impossible. The numerical method of finding the derivatives (8) for three-phase machines with PMs, based on the theory of invariant approximation of functions, is considered in [29]. For this problem, this method is extended to the case of DTP modular machines.

Therefore, to calculate the derivatives (8) at each point with seven coordinates $i_1, i_2, i_3, i_4, i_5, i_6, \gamma$, the following steps must be performed:

1. For a set of seven coordinates, form a Taylor matrix $\boldsymbol{T}$ of dimension 8 and find the inverse matrix $\boldsymbol{T}^{-1}$. This operation is performed once because the geometry of the kit remains the same for any machine mode of operation.

2. Since the coordinates differ significantly in their values, it is necessary to perform scaling. To do this, the beginning of the coordinate system is transferred to the point $i_1, i_2, i_3, i_4, i_5, i_6, \gamma$, and the coordinates of the 8-node set are calculated in the physical coordinate system, which corresponds to the geometry of the scaled set. Thus, the n-th node ($n = \overline{1,8}$) of this set is defined as

$$\begin{Vmatrix} i_{1,n} \\ i_{2,n} \\ i_{3,n} \\ i_{4,n} \\ i_{5,n} \\ i_{6,n} \\ \gamma_n \end{Vmatrix} = \begin{Vmatrix} m_{i_1} & & & & & & & \\ & m_{i_2} & & & & & & \\ & & m_{i_3} & & & & & \\ & & & m_{i_4} & & & & \\ & & & & m_{i_5} & & & \\ & & & & & m_{i_6} & & \\ & & & & & & m_{\gamma} & \end{Vmatrix} \cdot \begin{Vmatrix} x_{1,n} \\ x_{2,n} \\ x_{3,n} \\ x_{4,n} \\ x_{5,n} \\ x_{6,n} \\ x_{7,n} \end{Vmatrix} + \begin{Vmatrix} i_1 \\ i_2 \\ i_3 \\ i_4 \\ i_5 \\ i_6 \\ \gamma \end{Vmatrix}, \tag{9}$$

where diag $\left(m_{i_1}, m_{i_2}, m_{i_3}, m_{i_4}, m_{i_5}, m_{i_6}, m_{i_\gamma}\right)$ is the matrix of scale factors, which elements show how many units of a physical quantity (current, angle, etc.) contains a relative unit of the scalable set, $\left\|x_{1,n}, x_{2,n}, x_{3,n}, x_{4,n}, x_{5,n}, x_{6,n}, x_{7,n}\right\|^T$ is the column with the coordinates of the n node of the scaled set, and $\|i_1, i_2, i_3, i_4, i_5, i_6, \gamma\|^T$ is the column with the coordinates of the beginning of the coordinate system.

3. Calculate the discrete functions $\vec{\psi}$ and T_e for all nodes of the kit and form columns $\vec{\psi}_1, \vec{\psi}_2, \vec{\psi}_3, \vec{\psi}_4, \vec{\psi}_5, \vec{\psi}_6, \vec{T}_e$ from them.
4. Find the column of the scalable derivatives for the function ψ_1

$$\vec{c} = \boldsymbol{T}^{-1} \cdot \vec{\psi}_1 = \|c_1,\ c_2,\ c_3,\ c_4,\ c_5,\ c_6,\ c_7\|^T . \tag{10}$$

5. Determine its partial derivatives in physical coordinates:

$$\begin{gathered} \frac{\partial \psi_1}{\partial i_1} = \frac{c_1}{m_{i_1}}, \quad \frac{\partial \psi_1}{\partial i_2} = \frac{c_2}{m_{i_2}}, \quad \frac{\partial \psi_1}{\partial i_3} = \frac{c_3}{m_{i_3}}, \quad \frac{\partial \psi_1}{\partial i_4} = \frac{c_4}{m_{i_4}}, \\ \frac{\partial \psi_1}{\partial i_5} = \frac{c_5}{m_{i_5}}, \quad \frac{\partial \psi_1}{\partial i_6} = \frac{c_6}{m_{i_6}}, \quad \frac{\partial \psi_1}{\partial \gamma} = \frac{c_7}{m_{i_\gamma}}. \end{gathered} \tag{11}$$

6. Repeat steps 4 and 5 for the scalar functions $\psi_2, \psi_3, \psi_4, \psi_5, \psi_6$.
7. Fill the matrix (8) with the values.

Using the proposed algorithm, the elements of the differential inductance matrix (8) were calculated for the studied DTP PM machine. Figure 8 shows the

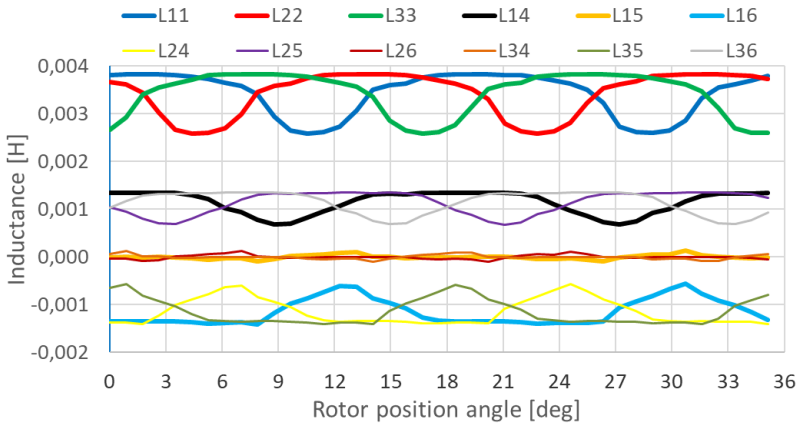

Figure 8: Dependences of the elements of the inductance matrix on the rotor position angle during idle

dependences of the self and some mutual differential inductances of the machine on the rotor position angle during idle.

As can be seen from the obtained results, the mutual inductances between the phases belonging to one module are practically absent. This is due to the specific location of the phase coils in accordance with the winding scheme, which provides a shift of the MMFs of individual modules, namely: between the phase coils of one module in the machine $Z/2p = 24/20$ are always coils belonging to another module.

The coefficient of mutual inductance close to zero is also inherent in phases that are shifted in space by 90°el. In a traditional three-phase machine, the mutual inductances are always negative. This means that the EMF of mutual induction between phases always reduces the value of the EMF of self-induction. This also occurs in the studied DTP PM machine, but only between the phases of the modules, which are shifted in space by 210°el. (1-6, 2-4, 3-5), while between the phases of the same name, which belong to different modules (1-4, 2-5, 3-6), there is a positive mutual inductive link.

The symmetry of the matrix of differential inductances is not violated, which can serve as additional proof of the mathematical correctness of the proposed algorithm for calculating the MMPs. The structure of the obtained matrix $\boldsymbol{L}$ is as follows

$$\boldsymbol{L} = \frac{\partial \vec{\psi}}{\partial \vec{i}} = \begin{Vmatrix} + & 0 & 0 & + & 0 & - \\ 0 & + & 0 & - & + & 0 \\ 0 & 0 & + & 0 & - & + \\ + & - & 0 & + & 0 & 0 \\ 0 & + & - & 0 & + & 0 \\ - & 0 & + & 0 & 0 & + \end{Vmatrix}, \tag{12}$$

where the signs “+” and “–” indicate the above features.

Figure 9 shows a comparative description of the four modes of operation of the studied DTP PM machine in terms of the influence of the parameters of these modes on the MMPs. The first mode is the idle (no load); the third – corresponds to the power supply of symmetrical three-phase current with the magnitude of 10 A system only of the first module, the second module is disconnected; the second and fourth modes – power supply of two modules were carried out simultaneously and symmetrically but at different values of current magnitude, 5 A and 10 A respectively.

The dependences in Fig. 9 show that, at the qualitative level, their nature has not changed, but there is some decrease in the average values of self and mutual differential inductances, which are nonzero, with increasing the load of machine modules. There is also a shift of the physical neutral in the direction of rotation of the inductor.

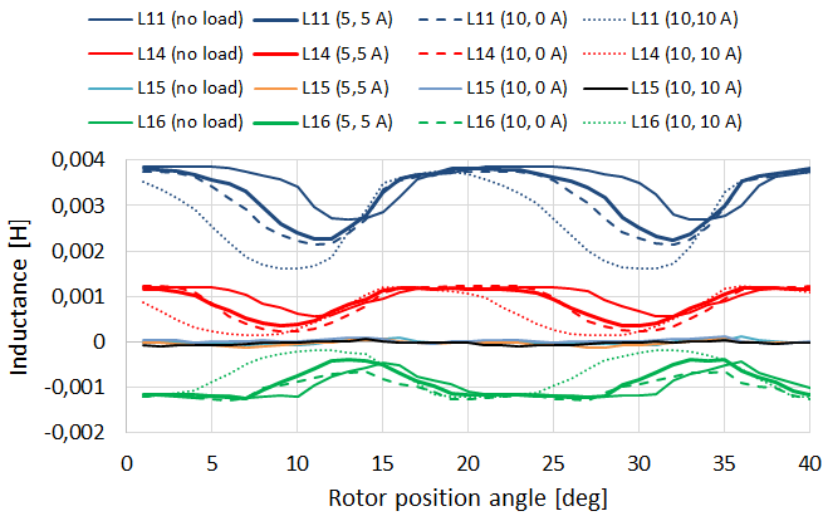

Figure 9: Comparison of the angular dependences of the self-differential inductance of phase 1 (L_{11}) and the related mutual inter-module differential inductances (L_{14}, L_{15}, L_{16}) of the studied DTP PM machine under different load modes of its modules

Summarizing the results of the analysis, it can be stated that the developed algorithm for calculating the MMPs of the DTP PM machine makes it possible to determine the elements of the matrix $\boldsymbol{L}$ in any mode of operation of the machine and at arbitrary combinations of independent variables. It adequately responds to their change and allows to identify features of complex relationships between the design parameters of such machines, taking into account the main factors influencing the technical and economic indicators, including: saturation of the magnetic circuit, arbitrary distribution of armature windings, real magnetic circuit configuration, etc.

3. Circuit-based mathematical model of the DTP PM machine in phase coordinates

In order to develop and study new modular electric drive systems based on the DTP PM machine, it is necessary to develop its high-speed in solving mathematical model, which is based on the description of electromagnetic processes by electric circuits. Since the DTP PM machine will work in the BLDC drive system, its operation should be modeled in phase coordinates, based on the obtained results of FEM modeling of the machine magnetic field.

In the created model we have accepted the following assumptions:

- The mathematical model of DTP PM machine is based on the improved well-known model of BLDC motor in phase coordinates with static inductances.
- As static self and mutual inductances are taken as determined by the developed algorithm respective dynamic inductances at the root mean square (rms) currents of 3 A for both machine modules, when the saturation of the magnetic circuits is minimal. Thus, the dependences of the self and mutual inductances on currents is not taken into account.
- The dependences of the self and mutual inductances on the angular position of the rotor is taken into account, because the studied PM machine has a sufficient polarity. However, this dependence, in order to simplify the model, is also taken at the rms currents of 3 A for both machine modules.
- The shape of the rotation EMFs consists of only the two largest harmonics – the first and the third.
- Both machine modules and their magnetic circuits are symmetrical.
- Losses in steel and permanent magnets are neglected.
- The influence of the cogging component of the torque is not taken into account.

Then, the voltage equilibrium in the six DTP phase circuits of the armature winding will be described by the following vector-matrix equation:

$$\vec{v} = \boldsymbol{R}\vec{i} + \boldsymbol{L}\frac{\mathrm{d}}{\mathrm{d}t}\vec{i} + \vec{e}\,, \tag{13}$$

where $\vec{v}$, $\vec{i}$, $\vec{e}$ are the vectors-columns of phase voltages, currents and EMFs, respectively, consisting of six elements, for each of the two sets the DTP armature winding, $\boldsymbol{R}$ is the diagonal matrix of six identical phase resistances R for each of the modules, $\boldsymbol{L}'$ is the matrix of static inductances.

According to the results of the FEM simulation of the magnetic field of the studied DTP PM machine, the matrix of differential inductances $\boldsymbol{L}$ has the structure (12). According to the above assumptions, the static inductance matrix $\boldsymbol{L}'$ of the studied DTP PM machine will look like

$$\boldsymbol{L}' = \begin{Vmatrix} L_{11}(\gamma) & 0 & 0 & L_{14}(\gamma) & 0 & L_{16}(\gamma) \\ 0 & L_{22}(\gamma) & 0 & L_{24}(\gamma) & L_{25}(\gamma) & 0 \\ 0 & 0 & L_{33}(\gamma) & 0 & L_{35}(\gamma) & L_{36}(\gamma) \\ L_{41}(\gamma) & L_{42}(\gamma) & 0 & L_{44}(\gamma) & 0 & 0 \\ 0 & L_{52}(\gamma) & L_{53}(\gamma) & 0 & L_{55}(\gamma) & 0 \\ L_{61}(\gamma) & 0 & L_{63}(\gamma) & 0 & 0 & L_{66}(\gamma) \end{Vmatrix}, \tag{14}$$

moreover on the principle of reciprocity $L_{ij}(\gamma) = L_{ji}(\gamma)$.

The angular dependences of the self and mutual static inductances that formulate the matrix (14) obtained by FEM simulation are shown in Fig. 10.

Shown in Fig. 10 dependencies are approximated by Fourier series, and, as studies have shown, the average value and the four harmonics of the series are sufficient with good accuracy for this model:

$$L(\gamma) = g_0 + g_1\cos(\gamma) + g_2\sin(\gamma) + g_3\cos(2\gamma) + g_4\sin(2\gamma) + g_5\cos(3\gamma) + g_6\sin(3\gamma) + g_7\cos(4\gamma) + g_8\sin(4\gamma), \tag{15}$$

where g_i are the obtained Fourier series coefficients.

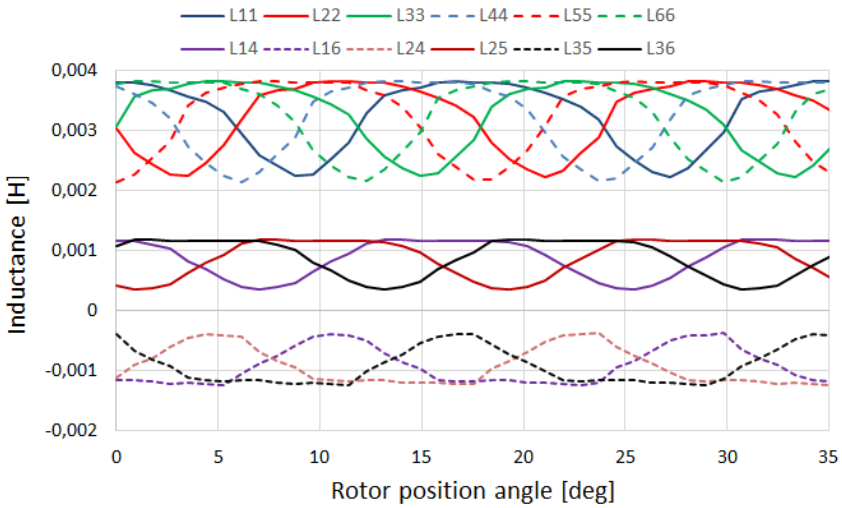

Figure 10: Accepted in the mathematical model dependences of self and mutual static inductances on the angle of the rotor position (independent from currents)

Figure 11 demonstrates the approximation by function (15) of the self-inductance L_{11} for the phase 1 and associated with the phase 1 the positive L_{14} and negative L_{16} mutual inductances.

The electromagnetic torque of the DTP PM machine can be expressed as

$$T_e = \frac{\left(\vec{e} \times \vec{i}\right)}{\omega}, \tag{16}$$

where $\left(\vec{e} \times \vec{i}\right)$ is the dot product of the EMF and armature current vectors.

For the simplest single-mass mechanical system with the total moment of inertia J_Σ with regard to the motor shaft, the equation of motion of the drive is

$$J_\Sigma \frac{\mathrm{d}\omega}{\mathrm{d}t} = T_e - T_L - b\omega, \tag{17}$$

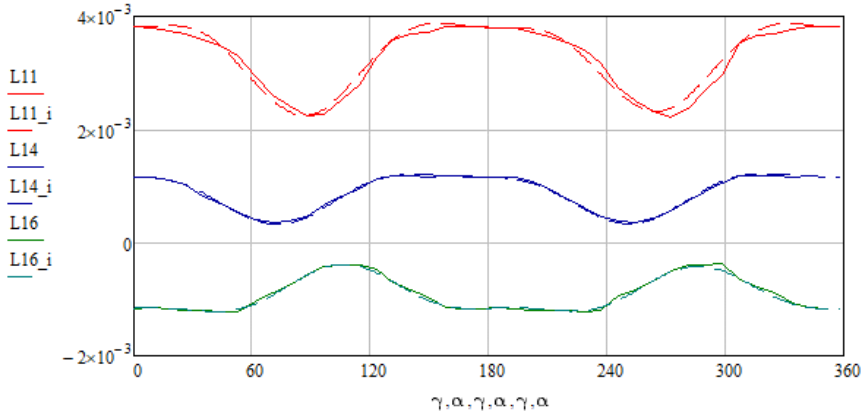

Figure 11: Comparison of the related to phase 1 angular dependencies of self and mutual inductances (solid lines) with their approximated by (15) functions (dashed lines)

where T_L is the load torque of the drive and b is the coefficient of viscous friction.

The position angle of the motor rotor is determined by integrating the angular velocity at zero initial conditions:

$$\gamma = \int \omega \mathrm{d}t \,. \tag{18}$$

The parameters of the elements of the voltage vector applied to the armature windings $\vec{v}$ in (13) depend on the method of controlling a DTP PM machine. In the case of BLDC with 120-degree switch conductivity [19], these parameters change six times over the period differently for each of the modules of the armature winding. Using the switches of VSIs (Fig. 1), at each time point, two phases of each module are connected in series to its DC bus, and one phase is disconnected. During phase switching, the current of the open phase continues to flow through freewheeling diodes and connected phases. Due to the complexity of the mathematical description of switching processes of each of the DTP PM machine modules, mathematical modeling of BLDC drive should be performed by computer simulation in Matlab/Simulink using available in the SimScape library virtual models of transistor bridges switching according to its six-step algorithms. For BLDC drive based on the DTP PM machine of asymmetric configuration with shifted on 30°el. armature winding, such algorithms are presented in Table 1.

Table 1: The order of six-step switching of the BLDC drive based on the DTP PM machine of asymmetric configuration with shifted on 30°el. sets of the armature winding

γ (°)	Switching states												γ (°)
	VSI 1						VSI 2						
	$S1_1$	$S1_2$	$S1_3$	$S1_4$	$S1_5$	$S1_6$	$S1_1$	$S1_2$	$S1_3$	$S1_4$	$S1_5$	$S1_6$	
0–30	1	1	0	0	0	0	1	1	0	0	0	0	0–30
30–60							1	0	0	1	0	0	30–60
60–90	1	0	0	1	0	0							60–90
90–120							0	0	1	1	0	0	90–120
120–150	0	0	1	1	0	0							120–150
150–180							0	0	1	0	0	1	150–180
180–210	0	0	1	0	0	1							180–210
210–240							0	0	0	0	1	1	210–240
240–270	0	0	0	0	1	1							240–270
270–300							0	1	0	0	1	0	270–300
300–330	0	1	0	0	1	0							300–330
330–360							1	1	0	0	0	0	330 – 360

4. Computer simulation of the DTP BLDC drive in Matlab/Simulink

The computer model of the DTP BLDC drive developed in the Matlab/Simulink environment is shown in Fig. 12. The model consists of two similar parts, which subsystems and main blocks are marked by indices 1 and 2. Each part includes an electromagnetic subsystem of the DTP PM machine – the PM Machine Module Subsystem, which switches by its six-switch VSI powered by its battery module B. The PWM Subsystem generates 120-degree switching signals based on the signals "pulses" produced by the Hall Subsystem based on the information of the rotor position angle. Given the asymmetric configuration of the two modules of the armature winding, the switching of the VSI2 is shifted by an angle $\pi/6$ relative to the VSI1 that ensures the operation of the switches of both inverters in accordance to Table 1. Both channels have a common reference of DC supply voltage U^*, which increases at a constant rate providing PWM control of the voltages coming from the batteries until the VSIs switches will open at the base frequency determined by the rotor angular velocity, and full batteries voltages apply to the sets of armature winding. The electromagnetic torques generated by the two machine modules are added, and the total electromagnetic torque is fed the common mechanical part of the drive, which is realized according to equations (17) and (18).

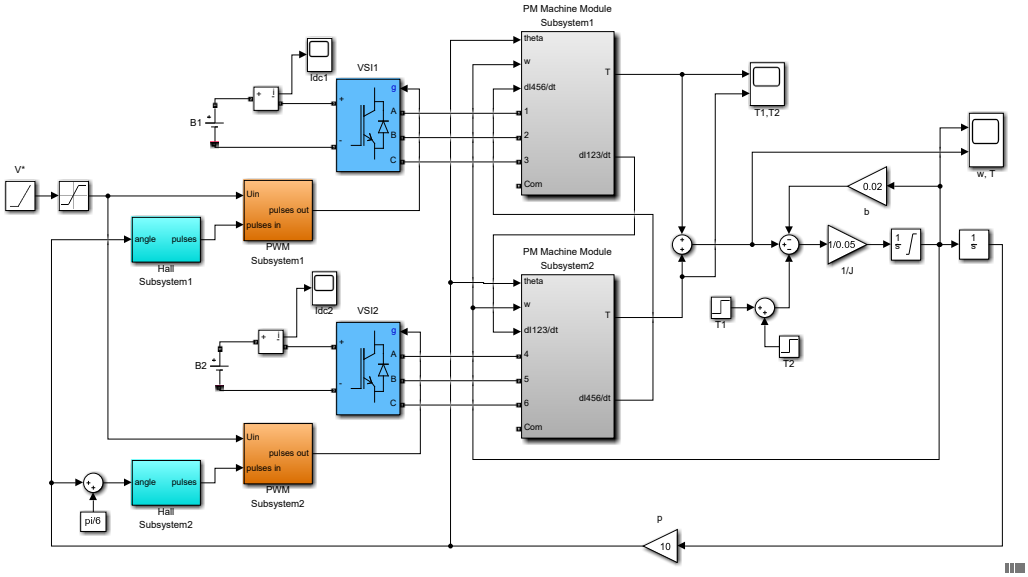

Figure 12: Computer mode of the DTP BLDC drive

In computer model shown in Fig. 12, the VSIs subsystems have been took from the SimScape library of Simulink and the PWM Subsystems and Hall Subsystems are the same as in the model given in [25]. The PM Machine Module Subsystems differ from the ones in [25] by angular dependences of self and mutual inductances and are realized as follow.

4.1. Model of the electromagnetic part of the studied DTP PM machine

The computer model of the electromagnetic part of the first DTP PM machine module, which is based on the mathematical model described in Section 3, is presented in Fig. 13. Its left part consists of three identical channels that integrate the equations of voltage balances (13) in three phases of this winding set. At the output of each channel, the value of the phase line current is obtained. Three current values form references for controlled current sources CCS1 – CCS3, which join the signals of the applied phase voltages with the virtual part of the power supply of the machine module from VSI. From these voltages at the input of the channels, the voltage drops on the active resistance of the winding R and the sums of the EMFs of rotation and the EMFs of mutual induction are subtracted. The values of the EMFs for three phases are formed in the EMF Subsystem and Mutual Induction Link Subsystem. The self-induction flux linkages obtained after integration in each channel are divided into self-static inductances, in which the angular dependences are formed by functional blocks L11, L22, L33, where the corresponding dependencies obtained by expressions

(15), are recorded. The obtained values of line currents are also used to calculate the electromagnetic torque by expression (16), and their discrete derivatives come to the output 2 of the subsystem and then go to the Mutual Induction Link Subsystem of another module to form there the EMFs of mutual induction.

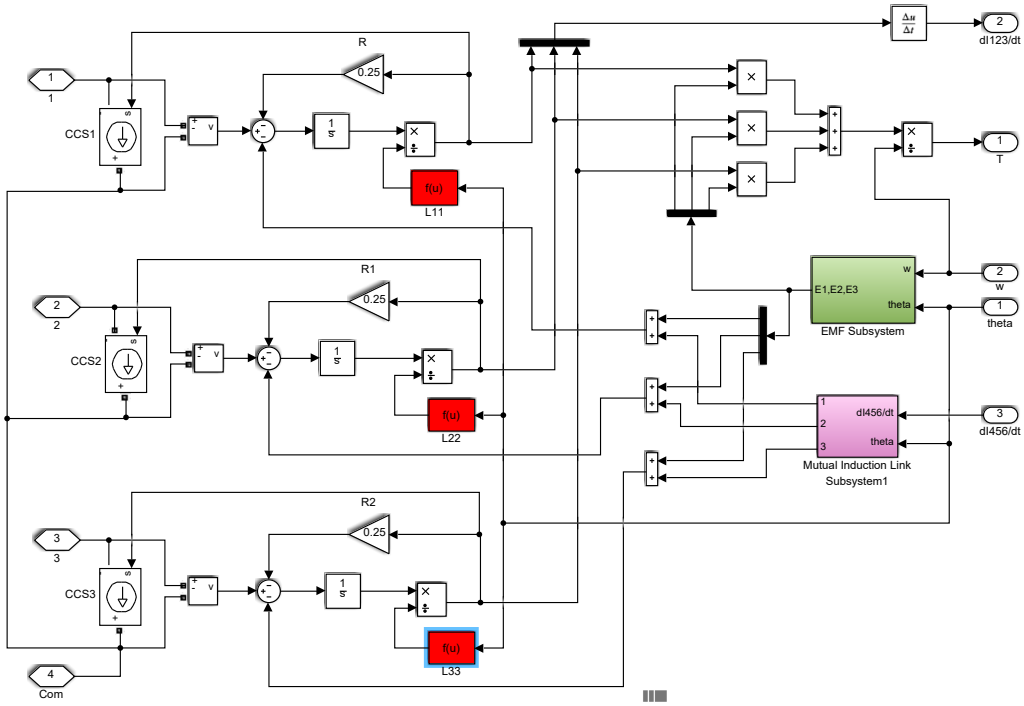

Figure 13: Computer model of the electromagnetic part of the first module of DTP PM machine

In the computer model of the EMF Subsystem for one machine module shown in Fig. 14, three Flux Linkage Shape Subsystems form angular dependences of phase flux linkages during idle as part of the first and third harmonics with total unit amplitude. Next, these dependencies are multiplied by the current value of the angular frequency w and the amplitude of the flux linkage caused by PMs F, as a result, the current values of the EMF of rotation of the machine module are obtained at the output of the subsystem.

In the computer model of the Mutual Induction Link Subsystem shown in Fig. 15 for the first machine module, the angular dependences of nonzero static mutual inductances are applied, which form the mutual inductance EMFs for this machine module at the output of this subsystem. The expressions for these static mutual inductances, which are written in the corresponding functional blocks f(u), are obtained as a result of approximation by expression (15) the dependences shown in Fig. 10.

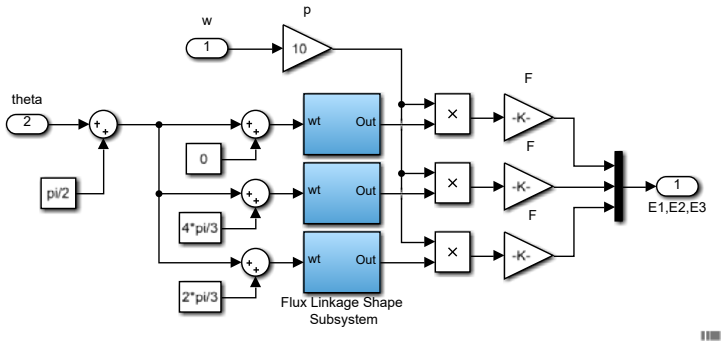

Figure 14: Computer model of the EMF Subsystem for one machine module

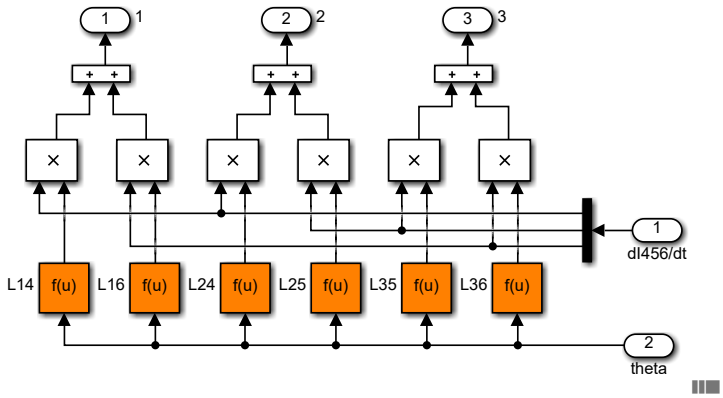

Figure 15: Computer model of the Mutual Induction Link Subsystem for the first machine module

Thus, in contrast to similar studies [30, 31], the model takes into account the dependences of self and mutual inductances on the angular rotor position that increases its accuracy.

The computer model of the electromagnetic part of the second module of the DTP PM machine differs from the similar model of the first module by shifting on the angle $\pi/6$ the phase EMFs of rotation in EMF Subsystem and by the topology of the Mutual Induction Link Subsystem according to the matrix of static inductances (14).

4.2. The results of computer simulation of the DTP BLDC drive work

4.2.1. Open-loop system

Figure 16 presents the waveforms of the main variables of the studied open-loop DTP BLDC drive obtained in the simulation of the model shown in Fig. 12. The voltages of both batteries in this experiment were equal and amounted to

25.5 V. By the time 0.08 s, the DC voltages applied to the armature windings of machine modules increase at a rump of 100 V/s due to PWM control. Next, the full voltages of the batteries are applied to the armature windings, and the switching of the windings takes place at the fundamental frequency. This is done in order to see the natural shapes of the line currents in the modules and to estimate the level of pulsations of the electromagnetic torque. At a time of 0.2 s, an additional load torque is applied to the rotor of the machine. As can be seen from Fig. 16b, the electromagnetic torques of each module have significant pulsations, at the level of 57% of the steady state. However, the pulsations of the electromagnetic torques generated by each of the machine modules, due to the asymmetric configuration of the machine, are in antiphase. Therefore, as can be seen from Fig. 16c, the total electromagnetic torque ripple of the DTP BLDC PM motor reduced to 16%.

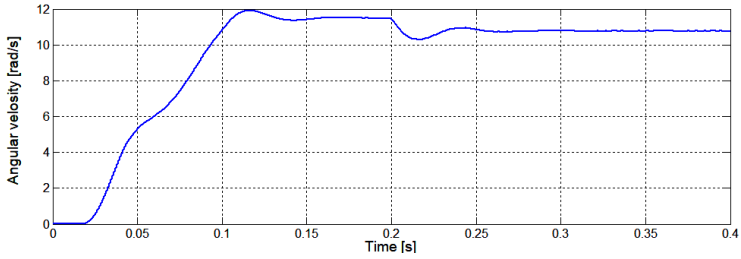

(a)

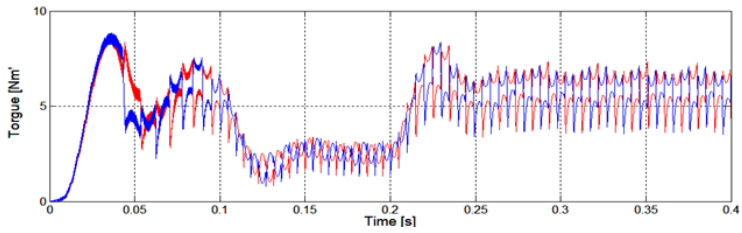

(b)

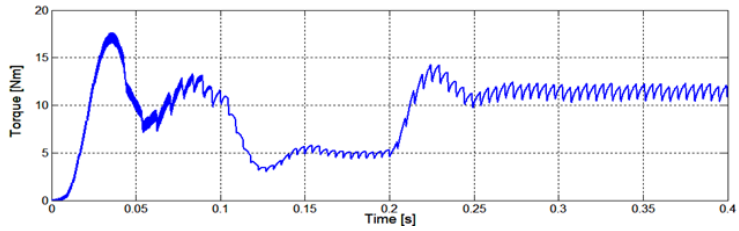

(c)

Figure 16: Waveforms of main variables of the studied open-loop DTP BLDC drive at start-up and abrupt loading: (a) angular velocity, (b) electromagnetic torques of two modules, (c) total electromagnetic torque

Figure 17a demonstrates the waveforms of the voltage and current of one phase, which show the significant voltage emissions associated with the switching moments of the windings in both machine modules. Due to the magnetic coupling between the windings, current changes in one winding generate EMFs of mutual induction in other windings. This causes the characteristic pulsations of line currents in each phase at intervals of 30°el. as can be seen from Fig. 17b, where the line currents in 1 and 4 phases shifted by 30°el. are shown.

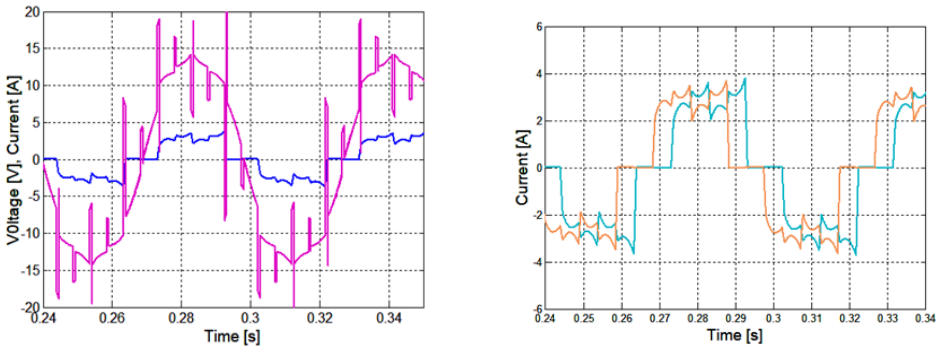

(a) (b)

Figure 17: Waveforms of the studied open-loop DTP BLDC drive: (a) voltage and current of one phase, (b) line currents in 1 and 4 phases

In the case of even a slight deviation of the DC values of the voltages applied to the two VSIs, the loading of the two machine modules is significantly different. This leads to a change in the shape of the line currents in the two modules, as well as to an increase in the total electromagnetic torque ripple. This explains the need for automatic control in closed-loop systems in order to equalize currents or electromagnetic torques in real drive systems, where the supply voltages of the modules are always not equal to each other [20].

4.2.2. Closed-loop control system

One of the simplest closed-loop control systems that can be applied to a DTP BLDC motor may be a system that has two control loops: the outer common loop of the angular speed control by a speed regulator and the inner loops of current control in each machine module by current regulators [32]. Automatic control of armature currents is easiest with PWM of the three lower switches of each VSI, because with 120-degree commutation mode these switches always work in one of the phases. For making the current control loops, in this system, the estimated current values of each winding set were obtained from current estimators. The latter measure currents in two phase winding of each set by current sensors and form from them the respective values of DC currents based on the gate signals

that control the VSIs [4]. The computer model of such a closed-loop control system of the DTP BLDC motor is shown in [25]. The closed two-loop control system has been created by using a proportional speed regulator SR ($k_P = 10$) and two PI current regulators CR ($k_P = 10$, $k_I = 500$).

Figures 18 and 19 show the same waveforms as Figs. 16 and 17, but for the closed-loop system of the studied DTP BLDC drive. As can be seen from these simulation results, the line currents control in both winding sets provides a

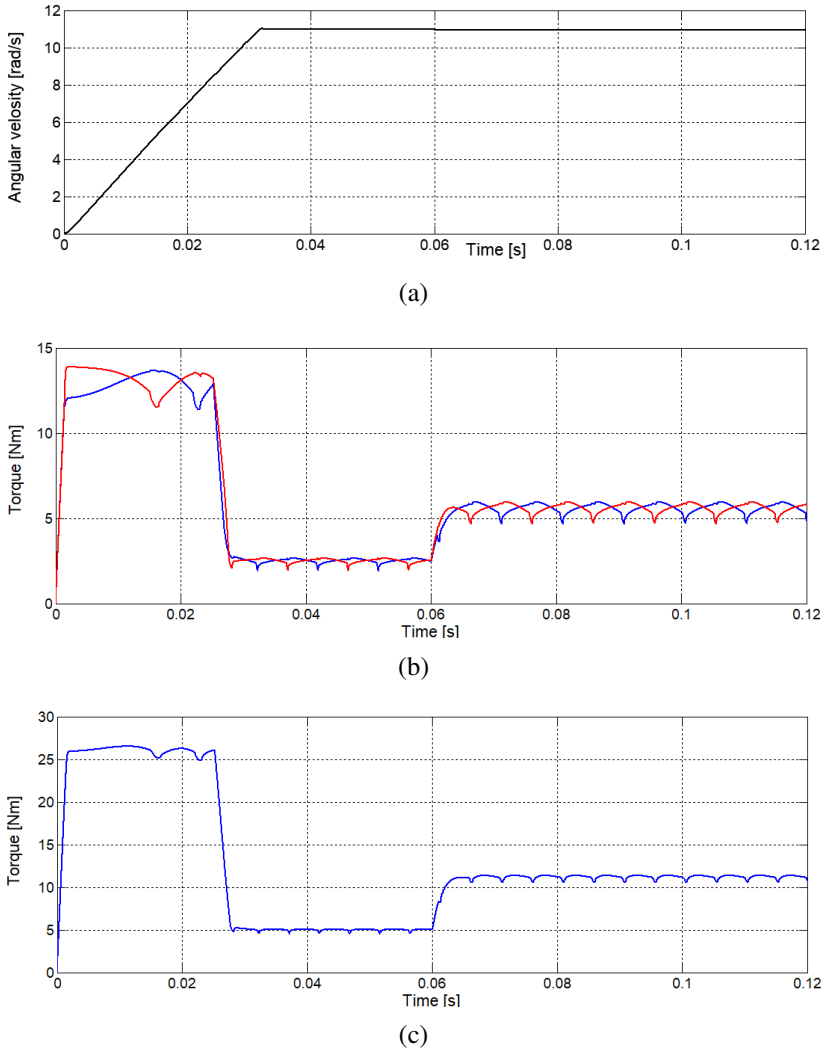

Figure 18: Waveforms of main variables of the studied closed-loop DTP BLDC drive at start-up and abrupt loading: (a) angular velocity, (b) electromagnetic torques of two modules, (c) total electromagnetic torque

significant reduction in the current pulsations and, accordingly, the pulsations of the electromagnetic torques. Thus, the pulsations of the electromagnetic torques generated by each of the modules are reduced to 20%, and in the drive as a whole – up to 10%. At the same time, the speed of regulation also increases and equality of currents and electromagnetic torques of both machine modules are provided even at considerable differences in levels of DC supply voltages of the VSIs.

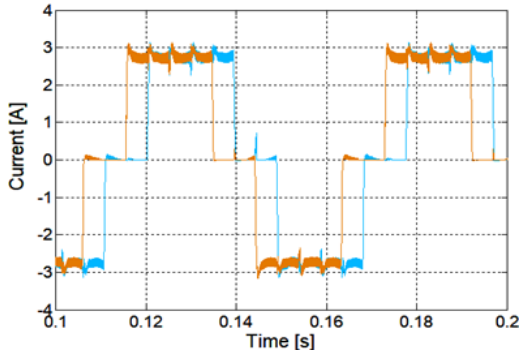

Figure 19: Waveforms of the line currents in 1 and 4 phases of the studied closed-loop DTP BLDC drive

5. Experimental verification of DTP BLDC PM motor model

In order to assess the adequacy of the constructed mathematical model of the DTP PM machine, experimental studies were performed with a mock-up sample of the asymmetric configuration machine with an external rotor, which photos are shown in Fig. 20.

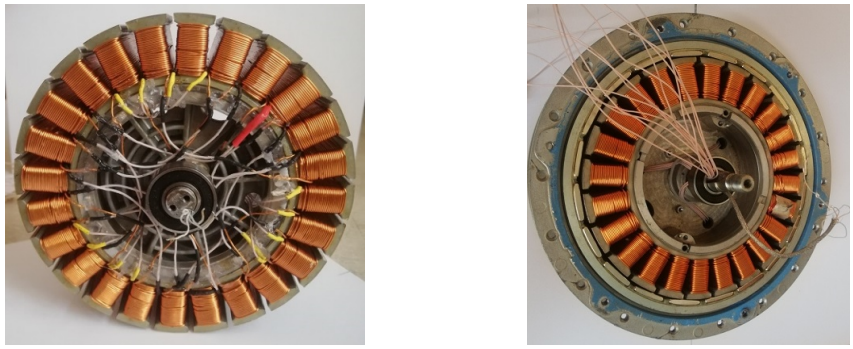

(a) (b)

Figure 20: Stator (a) and motor assembly (b) of the studied DTP PM machine

Six point sensors of the rotor position are required to implement a DLDC drive based on the studied DTP PM machine. For this purpose, a miniature absolute magnetic semiconductor encoder AS5045 with a 12-bit (4096 dots per revolution) code is used, which provides data transmission via a serial interface. This is a chip with integrated Hall elements, which is mounted on the end of the fixed stator shaft, as shown in Fig. 21a. The chip responds to the angle of rotation of a conventional bipolar magnet that rotates around its center. To implement this movement, an overhead coupling with an additional shaft is used. The coupling is mounted on the outer machine rotor, as shown in Fig. 21b. A cylindrical magnet is glued to the inner side of the shaft of the coupling, and a bearing is placed on its outer shaft. The bearing is fixed in the motor mounting bracket.

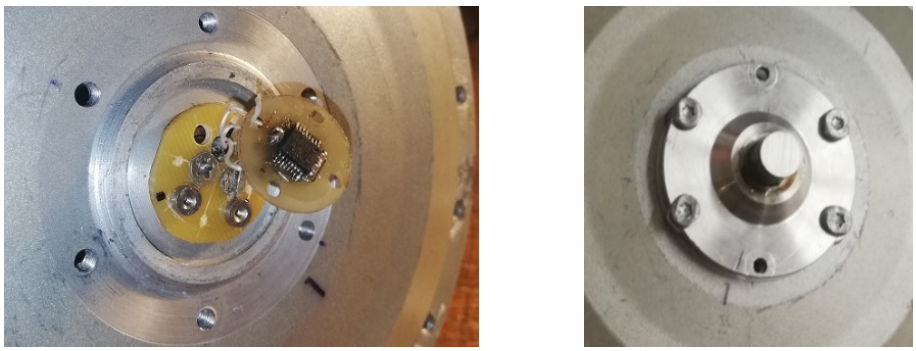

(a) (b)

Figure 21: Magnetic semiconductor encoder AS5045 (a) and coupling with additional shaft (b), which ensures the operation of the encoder

The electrical circuit of the encoder consists directly of the AS5045 chip and a separate ATmega8 microcontroller, which receives data on the rotor angular position from the AS5045 and transmits them via a serial interface to the microcontroller of the control system of the DLDC drive. The latter is a simple Arduino PRO mini Atmega168 microcontroller. From the signals of the encoder, those are selected that allow the microcontroller to perform the six-step 120-degree switching synchronized with the EMFs of two sets of the DTP armature winding. The built-in timers of the controller counter made it possible to create 6 PWM signals supplied to the IR2104 drivers, which control 12 MOSFET transistors IRF3205 of two VSIs. The operating frequency of the PWM was chosen as 16 MHz / 512 = 31.25 kHz, where 16 MHz is the microcontroller carrier frequency.

The whole experimental stand is shown in Fig. 22. The power supply of both VSIs was carried out from two blocks of stabilized voltage PS-305D. Galvanic isolation of the controller from the inverter drivers was provided through the

PC817 optocouplers. The studied DTP PM machine is interlocked to a DC generator through a toothed belt mounted on the outer rotor of the studied machine. The generator is loaded on a resistor that regulated the loading torque of the drive.

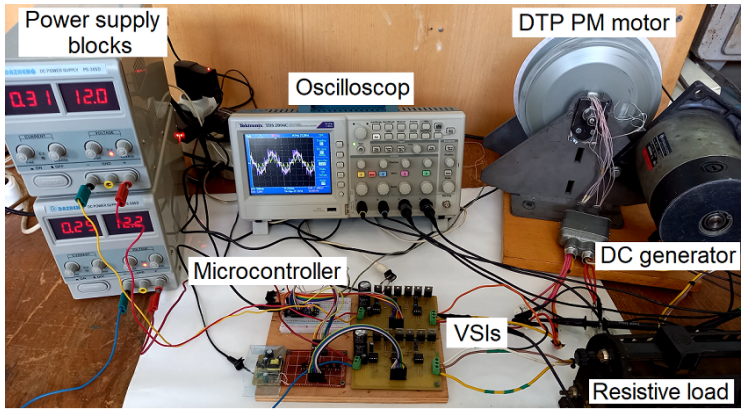

Figure 22: Experimental stand of the open-loop DTP BLDC drive

Figure 23 shows the obtained experimentally oscillograms of the studied open-loop DTP BLDC drive at the same supply voltage, angular speed, and load torque as in the simulation results presented in Fig. 17. Comparison of these two results shows their very good coincidence that indicates about sufficient adequacy of the mathematical model of the studied DTP PM machine developed in Section 3.

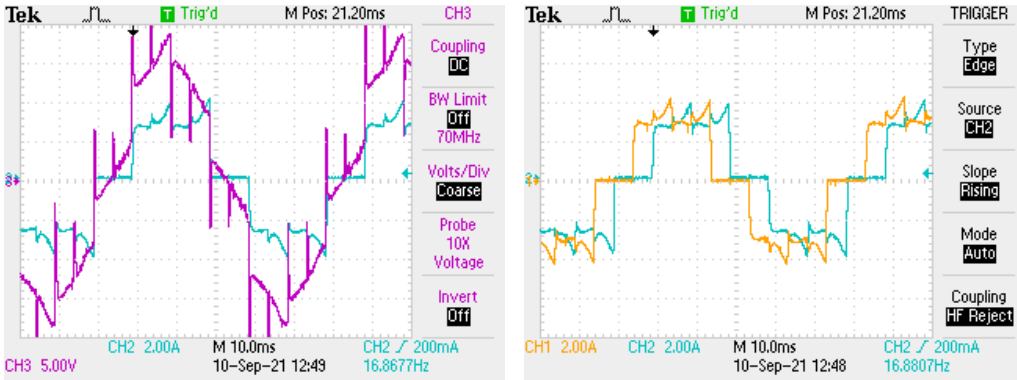

(a) (b)

Figure 23: scillograms of the studied open-loop DTP BLDC drive: (a) voltage and current of one phase, (b) line currents in 1 and 4 phases

6. Conclusions

Due to the mass production of EVs of different classes and purposes, there is a problem of correcting the traditional approaches to separate design of their main subsystems. Therefore, integration of the main subsystems of the EV powertrain system based on the universal principle of its configuration, construction of interconnections between these subsystems and their control is a promising research direction. The proposed modular approach to the configuration of powertrain systems simplifies and accelerates the EVs design, unifies components, and increases efficiency and reliability. A DTP PM motor is one of the examples of the modular approach, because it allows combining modular power supply, modular power convertor, modular electric machine, and special control and energy management methods.

Thanks to the results obtained in field research, the developed computer model of DTP PM machine futures increased precision as well as fast simulation capability. Conducted experiments verified a sufficient accuracy of the created model for conducting further research. BLDC drives based on the DTP PM machine of asymmetrical structure is noted by simplicity, high efficiency, fault tolerance, a low ripple of the total electromagnetic torque, as well as the possibility of developing the new configurations of electric drive with different level of power supply modularity and control possibility.

References

[1] T.A. Skouras, P.K. Gkonis, C.N. Ilias, P.T. Trakadas, E.G. Tsampasis and T.V. Zahariadis: Electrical vehicles: current state of the art, future challenges, and perspectives. *Clean Technologies*, **2**, (2020), 1–16. DOI: 10.3390/cleantechnol2010001.

[2] A. Stippich, C.H. van der Broeck, A. Sewergin and A.H. Wienhausen: Key components of modular propulsion systems for next generation electric vehicles. *CPSS Transactions Power Electronics and Applications*, **2**, (2017), 249–258. DOI: 10.24295/CPSSTPEA.2017.00023.

[3] A. Galassini, A. Costabeber, C. Gerada, G. Buticchi and D.A. Barater: Modular speed-drooped system for high reliability integrated modular motor drives. *IEEE Transactions Industry Application*, **52**, (2016), 3124–3132. DOI: 10.1109/TIA.2016.2540608.

[4] I. Shchur and V. Turkovskyi: I ntegrated system of modular power supply and multilevel control of brushless DC motor for electric vehicles. *Naukovyi*

Visnyk Natsionalnoho Hirnychoho Universytetu, **6**, (2020), 107–115. DOI: 10.33271/nvngu/2020-6/068.

[5] A. Salem and M.A. Narimani: Review on multiphase drives for automotive traction applications. *IEEE Transactions Transportation Electrification*, **5**, (2019), 1329–1348. DOI: 10.1109/TTE.2019.2956355.

[6] F. Barrero and M.J. Duran: Recent advances in the design, modeling, and control of multiphase machines, Part I. *IEEE Transactions Industrial Electronics*, **63**(1), (2015), 449–458. DOI: 10.1109/TIE.2015.2447733.

[7] A. Negahdari, A.G. Yepes, J. Doval-Gandoy and H.A. Toliyat: Efficiency enhancement of multiphase electric drives at light-load operation considering both converter and stator copper losses. *IEEE Transactions Power Electronics*, **34**, (2019), 1518–1525. DOI: 10.1109/TPEL.2018.2830310.

[8] V.I. Patel, J. Wang, D.T. Nugraha, R. Vuletić and J. Tousen: Enhanced availability of drivetrain through novel multiphase permanent-magnet machine drive. *IEEE Transactions Industrial Electronics*, **63**(1), (2016), 469–480. DOI: 10.1109/TIE.2015.2435371.

[9] W. Zhao, L. Xu and G. Liu: Overview of permanent-magnet fault-tolerant machines: Topology and design. *CES Transactions Electrical Machines and Systems*, **2**, (2018), 51–64. DOI: 10.23919/TEMS.2018.8326451.

[10] M. Zabaleta, E. Levi and M. Jones: Modelling approaches for an asymmetrical six-phase machine. *2016 IEEE 25th International Symposium on Industrial Electronics (ISIE)*, Santa Clara, CA, USA, (2016), 173–178. DOI: 10.1109/ISIE.2016.7744885.

[11] P. Zheng, F. Wu, Y. Lei, Y. Sui and B. Yu: Investigation of a novel 24-slot/14-pole six-phase fault-tolerant modular permanent-magnet in-wheel motor for electric vehicles. *Energies*, **6**, (2013), 4980–5002. DOI: 10.3390/en6104980.

[12] G.J. Li, B. Ren and Z.Q. Zhu: Design guidelines for fractional slot multiphase modular permanent magnet machines. *IET Electric Power Applications*, **11**, (2017), 1023–1031. DOI: 10.1049/iet-epa.2016.0616.

[13] Y. Yokoi, T. Higuchi and Y. Miyamoto: General formulation of winding factor for fractional-slot concentrated winding design. *IET Electric Power Application*, **10**, (2016), 231–239. DOI: 10.1049/iet-epa.2015.0092.

[14] S. Kallio, M. Andriollo, A. Tortella and J. Karttunen: Decoupled d-q model of double-star interior-permanent-magnet synchronous machines.

IEEE Transactions Industrial Electronics, **60**, (2013), 2486–2494. DOI: 10.1109/TIE.2012.2216241.

[15] D. Boudana, L. Nezli, A. Tlemçani, M. Mahmoudi, M. Djemai and M. Tadjine: Backstepping/DTC control of a double star synchronous machine drive. *Archives of Control Sciences*, **2**, (2010), 227–247. DOI: 10.2478/v10170-010-0015-6.

[16] S. Kallio, J. Karttunen, P. Peltoniemi, P. Silventoinen and O. Pyrhönen: Determination of the inductance parameters for the decoupled d–q model of double-star permanent-magnet synchronous machines. *IET Electric Power Application*, **8**, (2014), 39–49. DOI: 10.1049/iet-epa.2013.0195.

[17] I. Zoric, M. Jones and E. Levi: Arbitrary power sharing among three-phase winding sets of multiphase machines. *IEEE Transactions Industrial Electronics*, **65**(2), (2018), 1128–1139. DOI: 10.1109/TIE.2017.2733468.

[18] Y. Hu, Z.Q. Zhu and M. Odavic: Comparison of two-individual current control and vector space decomposition control for dual three-phase PMSM. *IEEE Transactions Industry Applications*, **53**(5), (2017), 4483–4492. DOI: 10.1109/TIA.2017.2703682.

[19] S.A.KH. Mozaffari Niapour, GH. Shokri Garjan, M. Shafiei, M.R. Feyzi, S. Danyali and M. Bahrami Kouhshahi: Review of permanent-magnet brushless DC motor basic drives based on analysis and simulation study. *International Review of Electrical Engineering (I.R.E.E.)*, **9**, (2014), 930–957. DOI: 10.15866/iree.v9i5.827.

[20] M. Ruiqing, L. Weiguo, L. Guangzhao and H. Yashan: The balanced current control of dual-redundancy permanent magnetic brushless DC motor. *2005 International Conference on Electrical Machines and Systems*, Nanjing, China, (2005), 475–479. DOI: 10.1109/ICEMS.2005.202573.

[21] Z. Luo, D. Liang and W. Ding: Dynamic modeling and characteristics analysis for dual-redundancy PM brushless DC servo system. *2011 International Conference on Electrical Machines and Systems*, Beijing, China, (2011). DOI: 10.1109/ICEMS.2011.6073881.

[22] Z. Fu, J. Liu and Z. Xing: Performance analysis of dual-redundancy brushless DC motor. *Energy Reports*, **6**, (2020), 829–833. DOI: 10.1016/j.egyr.2020.11.125.

[23] H. Yan, Y. Xu, J. Zou, B. Wang and S. Jiang: A maximum current sharing method for dual-redundancy brushless DC Motor control. *2014 17th International Conference on Electrical Machines and Systems*

(ICEMS), Hangzhou, China, (2014), 1057–1061. DOI: 10.1109/ICEMS.2014.7013634.

[24] C. Bian, X. Li and G. Zhao: The peak current control of permanent magnet brushless DC machine with asymmetric dual-three phases. *CES Transactions Electrical Machines and Systems*, **2**, (2018), 29–135. DOI: 10.23919/TEMS.2018.8326459.

[25] I. Shchur and D. Jancarczyk: Electromagnetic torque ripple in multiple three-phase brushless DC motors for electric vehicles. *Electronics*, **10**(24): 3097, (2021). DOI: 10.3390/electronics10243097.

[26] P. Bogusz, M. Korkosz and J. Prokop: A study of dual-channel brushless DC motor with permanent magnets. *2016 13th Selected Issues of Electrical Engineering and Electronics (WZEE)*, Rzeszow, Poland, (2016). DOI: 10.1109/WZEE.2016.7800189.

[27] O. Makarchuk, B. Kharchyshyn and L. Kasha: Analysis of the magnetomechanical characteristic of double three-phase PMSM. *2021 IEEE 3d Ukraine Conference on Electrical and Computer Engineering (UKRCON)*, Lviv, Ukraine, (2021), 333–338. DOI: 10.1109/UKRCON53503.2021.9575684.

[28] M. Lis and O. Makarchuk: Model matematyczny układu nadprądowego z silnikiem PMSM zasilanym ze źródła napięcia sinusoidalnego. *Przegląd Elektrotechniczny*, **12**, (2013), 211–214.

[29] O. Makarchuk: Methods and Principles of Creating of High-Speed Brushless Electric Machines with Permanent Magnets. *Dr Sci. Thesis, Lviv Polytechnic National University*, Lviv, Ukraine, (2017), 394 p.

[30] M. Gołębiowski, A. Smoleń, L. Gołębiowski and D. Mazur: Functional simulation model of the axial flux permanent magnet generator. *Archives of Electrical Engineering*, **67**(4), (2018), 857–868. DOI: 10.24425/aee.2018.124745.

[31] L. Gołębiowski, M. Gołębiowski and B. Kwiatkowski: Optimal control of a doubly fed induction generator of a wind turbine in island grid operation. *Energies*, **14**(23), 7883, (2021). DOI: 10.3390/en14237883.

[32] G. Sieklucki, A. Bisztyga, R. Sykulski, A. Zdrojewski and T. Orzechowski: Discrete-time switching state-space controller of DC drive. *Archives of Control Sciences*, **23**(3), (2013), 333–349. DOI: 10.2478/acsc-2013-0020.